



Title	Evolution of the Texture along the EPICA Dome C Ice Core
Author(s)	Durand, Gaël; Svensson, Anders; Persson, Asbjørn; Gagliardini, Olivier; Gillet-Chaulet, Fabien; Sjolte, Jesper; Montagnat, Maurine; Dahl-Jensen, Dorthe
Citation	低温科学, 68(Supplement), 91-105 Physics of Ice Core Records II : Papers collected after the 2nd International Workshop on Physics of Ice Core Records, held in Sapporo, Japan, 2-6 February 2007. Edited by Takeo Hondoh
Issue Date	2009-12
Doc URL	<a href="http://hdl.handle.net/2115/45436">http://hdl.handle.net/2115/45436</a>
Type	bulletin (article)
Note	I. Microphysical properties, deformation, texture and grain growth
File Information	LTS68suppl_009.pdf



[Instructions for use](#)

# Evolution of the Texture along the EPICA Dome C Ice Core

Gaël Durand \*, Anders Svensson \*, Asbjørn Persson \*, Olivier Gagliardini \*\*, Fabien Gillet-Chaulet \*\*, Jesper Sjolte \*, Maurine Montagnat \*\*, Dorthe Dahl-Jensen \*

\* *Niels Bohr institute, Ice and Climate Group, University of Copenhagen, Denmark. Contact author: gd@gfy.ku.dk.*

\*\* *Laboratoire de Glaciologie et de Géophysique de l'environnement, Saint-Martin d'Hères, France.*

**Abstract:** New measurements of ice texture made along the EPICA Dome C ice core, together with a review of previous studies of fabric and microstructure, are presented. Mean grain size increases steadily with age, and so depth. However, sharp decreases are observed contemporary with each climatic termination. These sharp decreases are believed to be mainly driven by the change in dust content between glacial and interglacial periods. C-axes steadily clustered with depth toward a vertical single maximum. However, a sharp clustering of the fabric is observed during termination II ( $\approx 1750$  m), suggesting the presence of shear in the upper part of the core. Moreover, below 2812 m, large variations of the fabric are observed from sample to sample. Migration recrystallization may affect the ice polycrystal for the lowest part of the core.

**Key words:** EPICA Dome C ice core, texture, anisotropy, recrystallization processes.

## 1 Introduction

Ice cores studies over the last decades have considerably enhanced our understanding of the nature of climate, showing, amongst other things, the correlation of the atmospheric composition of greenhouse gases with air temperature [1]. A new ice core has recently been drilled within the European Project for Ice Coring in Antarctica (EPICA) at Dome C in Antarctica ( $75^{\circ}06'S$ ,  $123^{\circ}21'E$ , 3233 m above sea level) reaching a depth of 3259.72 m. Analysis of the upper 3139 m of this core has pushed paleoclimate records in ice cores back to 800 kyr [2]. Besides this increase in the age of ice core records, also the analytical methods applied on ice cores have been strongly improved. For example, high resolution measurements have enabled the identification of seasonal variations in cores from sites with high accumulation rates (NorthGRIP, Greenland, [3]). However, stratigraphic disturbances in the deepest part of the ice cores drilled close to the summit of the Greenland ice sheet (GRIP and GISP2) have been reported [4, 5]. Small

scale folds have been observed which alter the stratigraphy at centimeter scale [GISP2, Greenland, 5], and, in some cases, even the large scale stratigraphic order of ice layers representing thousands of years can be disturbed [Vostok, Antarctica, 6]. Therefore, in order to obtain a fully confident interpretation of the paleoclimatic records in ice cores, the structural properties of the ice cores have also to be investigated.

The study of the ice polycrystal is a good candidate to detect strain heterogeneities and to get an understanding of the deformation history. Ice crystals are outstandingly anisotropic as deformation parallel to the basal planes (perpendicular to its  $c$  axis) is several orders of magnitude easier compared to any other direction [7]. As a consequence, under deformation, the  $c$  axes in the ice polycrystal rotate towards compression axes and away from tensional axes [8, 9]. Due to this, the  $c$  axes distribution (referred to as fabric in the following) both reflects the deformation history of the ice and determines the hardness of the ice with respect to further deformation. A thorough understanding of the fabric evolution in the ice sheet is, therefore, of primary importance to correctly interpret and simulate the ice flow [10].

Another very important aspect of the ice polycrystal is the microstructure, *i.e.* the grain boundary network. As observed in many ice cores, the mean crystal size shows abrupt variations in phase with climatic changes [11, 12]. Thus, mean grain size variations provide a valuable mark of rapid climate changes. Moreover, Cuffey et al. [13] have shown that the grain size may influence the strain-rate and lead to shear strain rate enhancement in ice accumulated during glacial periods (see the review of Paterson [14]). Finally, Durand et al. [15] have shown that the microstructure geometry also records the deformation history and may reveal strain heterogeneities.

The purpose of this paper is to present a review of the existing texture studies (both microstructure and fabric) of the EPICA Dome C (EDC) ice core, and to present new and more robust texture measurements, which allow us to improve the understanding of past ice sheet deformation in the vicinity of EDC. In section 2, we describe the basic mechanisms that affect the texture in ice sheets. Section 3 presents the parameters used to characterize the texture and details the different results. Section 4 discusses both

the microstructure and fabric evolutions, with particular emphasis on mean grain size variations and the sudden changes observed in the fabric.

## 2 Mechanisms affecting texture development

### 2.1 Deformation

The ice crystal has a hexagonal crystallographic structure and its orientation can be specified by its  $c$  axis which is perpendicular to the basal planes. Dislocation glide along the basal planes dominates ice crystal deformation and confers a strong anisotropy to the crystal [7]. Due to this strong anisotropy of the crystal,  $c$  axes rotate toward compressional axes and away from tensional axes [8, 16, 9]. The sketches in Figure 1 summarize the texture evolution under uniaxial compression.

However,  $c$ -axes rotation induced by strain is not the only process that affects the texture and several recrystallization processes have to be taken into account to correctly interpret texture evolution.

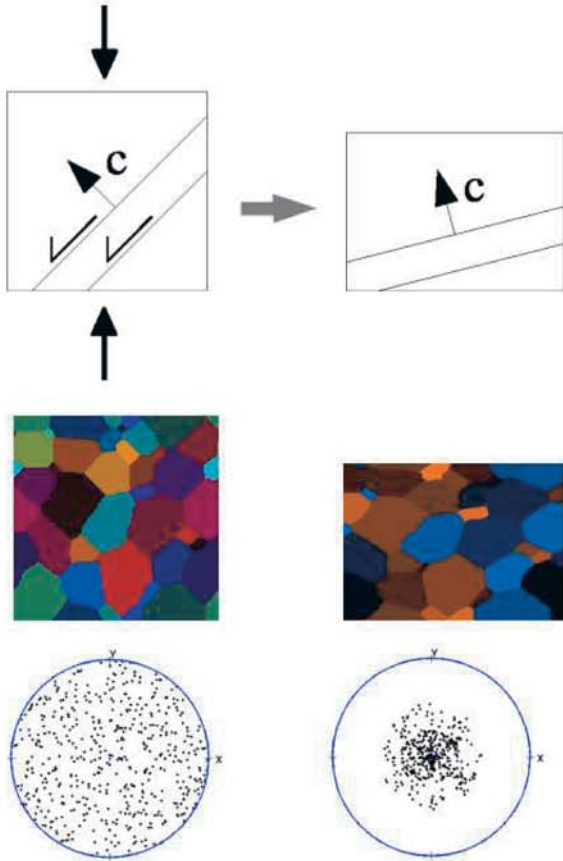


Figure 1: Sketches presenting the effect of uniaxial compression on an ice polycrystal. Due to strong crystal anisotropy,  $c$ -axes rotate toward the compressional axis. For the EDC case, compression direction corresponds to the in-situ vertical. Then, after deformation  $c$ -axes will appear clustered around the vertical (center of classical Schmidt projection), and grains become more elongated on the extension direction.

## 2.2 Recrystallization processes

### 2.2.1 Normal grain growth

In polycrystalline materials, the normal grain growth process is driven by the decrease of the total grain boundary energy within the material. Assuming that the grain boundary is a part of a sphere, and ignoring the environment of the grain, Burke and Turnbull [17] established that the boundary velocity  $v$  is inversely proportional to the grain radius. Further, assuming that  $v$  is proportional to  $dR/dt$ , they deduced that:

$$\frac{dR}{dt} = \frac{K}{R} \quad (1)$$

where  $K$  is an Arrhenius temperature-dependent constant. Integration of Equation (1) gives the classical parabolic grain growth law  $R^2 = R_0^2 + Kt$ , where  $R_0$  is the initial grain radius. Other approaches, like mean field assumptions [18], Monte Carlo simulations [19] or vertex modeling [20] give similar grain growth law exponents for the mean grain radius evolution of an assemblage of grains. Such a steady evolution is observed in the upper part of ice-sheets, with a slightly higher exponent  $m \simeq 3$  compared to the theoretical one (see *e.g.* Thorsteinsson et al. [21]). However, the grain evolution is clearly affected by other processes than normal grain growth, as a decrease of the mean grain size can be observed at the LGM-Holocene transition (termination I) in several ice cores (amongst others Vostok [22], GRIP [21]). Note also that Durand et al. [12] attribute the discrepancy between theoretical and measured exponent  $m$  to the effect of bubbles pinning.

Normal grain growth can be affected by the effect of extrinsic materials, that is in the case of polar ice: microparticles and bubbles through a pinning effect or soluble impurities through a drag effect. A review of the different mechanisms affecting normal grain growth has been proposed by Alley et al. [23]. An extensive debate has then followed to discriminate which mechanism is predominant in polar ice sheets and could explain the observed decrease at termination I [11, 24, 25, 26, 27, 28]. In the light of a detailed grain size record from the EDC core, Durand et al. [12] have reviewed the different arguments and conclude that the predominant impact is attributed to the pinning of grain boundaries by insoluble dust particles. In that case, Equation (1) can be modified as follows [29]:

$$\frac{dR}{dt} = K \left( \frac{1}{R} - \frac{1}{R_z} \right) \quad (2)$$

where  $R_z$  is a limiting grain size, that depends on the dust content of the ice and on the size of dust particles. The location of the particles is also a determinant parameter. Indeed, for a given dust particle size distribution,  $R_z$  is much lower if the particles are preferentially distributed along grain boundaries compared to randomly distributed particles within the ice matrix (see Durand et al. [12] for details). A nonlinear decay of the grain growth rate follows from equation (2):  $dR/dt$  progressively decreases

toward zero as the grain size approaches  $R_z$ . It is also worth mentioning that if grain boundaries are not pinned, normal grain growth always take place.

Whereas the normal grain growth obviously affects the grain size, it is believed that it does not influence fabrics development [16].

### 2.2.2 Rotation Recrystallization

Rotation recrystallization or polygonization signifies the splitting of grains into smaller grains. Because different parts of a grain are subject to different stresses induced by grain-grain interactions, dislocations group into walls (sub-boundaries) that divide the grains into less distorted regions. The misorientation between sub-grains increases as deformation proceeds, and sub-boundaries become true grain boundaries (the distinction between sub-grains and grains is arbitrary).

From the description of the mechanism, rotation recrystallization decreases the average grain growth rate of the polycrystal. It is believed that under some conditions, rotation recrystallization counteracts normal grain growth, and that it can explain the constant mean grain size that is observed in several ice cores (among others Byrd [30], GRIP [21], NorthGRIP [31]).

As new grains form by progressive rotation recrystallization, their orientation is close to the grain from which they form. Thus, the occurrence of rotation recrystallization can be determined by comparing the population of low-angle grain boundaries within the texture with that of a reshuffled texture [32, see also Section 3.2]. Moreover, from discrepancies between model results and observations along the GRIP core, Castelnau et al. [33] suspected rotation recrystallization to slow down the fabric strengthening under uniaxial compression.

### 2.2.3 Migration Recrystallization

Migration recrystallization is the nucleation of new dislocation free grains and rapid migration of their boundaries at the expense of strained grains. This process occurs in the very bottom part of ice sheets if the following conditions are fulfilled: (i) the temperature exceeds  $-10^\circ\text{C}$  and (ii) the driving force for the initiation of the migration recrystallization is reached [34].

The fast grain boundary migration associated with migration recrystallization leads to the formation of large interlocking grains that deeply affects the fabric. For normal grain growth and rotation recrystallization the fabric is strain induced, whereas under migration recrystallization, the resulting fabric is imposed by the state of stress [35]. Jacka and Maccagnan [36] have shown that under uniaxial compression, the  $c$  axes pattern resulting from migration recrystallization is a circular gridle at about  $30^\circ$  from the compressional axis. Note however that strain rates in laboratory experiments are orders of magnitude larger than in ice-sheets. Finally, Alley et al. [30] suggested that an over-representation of grains at high angle

to their neighbours could result from migration recrystallization. However, to our knowledge, this has never been measured in ice cores.

## 3 Methods and results

### 3.1 New measurements of the complete texture

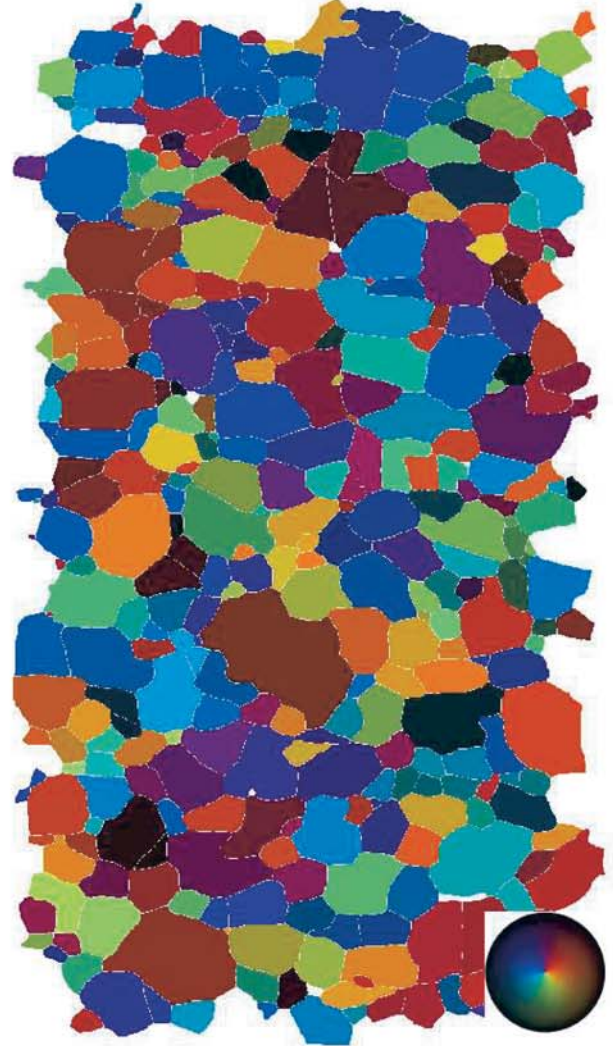


Figure 2: *Texture of a thin section sampled at 1767.8 m depth. The grain boundaries appear in white, and each grain within the microstructure has a color that specifies its  $c$  axis orientation. The polar plot projection on the bottom right corner specifies the relation between colors and  $c$  axis orientations. Note that the vertical axis of the image corresponds to the in-situ vertical axis*

Automatic Ice Texture Analyzers (AITAs) have been recently developed [37, 38, 39], which has lead to a large improvement in the polycrystal description. Indeed, several thousands of grains can easily be measured leading to improved statistical significance of the measurements. Moreover, both the microstructure and the fabric (*i.e.* the texture) are measured at the same time allowing the definition of more robust parameters and more complex analyses. For example, this allows us to investigate

the relation between neighbouring grains [40]. Accounting for the higher quality measurements offered by automatic techniques, a complete texture profile of the EDC core was measured from 214 m to 3133 m depth. Four cm wide and 11 cm high vertical thin sections (parallel to the core axis) were prepared using standard procedures (recalled in Durand et al. [40]). In the depth interval previously studied by Wang et al. [41] (from 100 down to 1500 m) thin sections were sampled only each 50 m. The sampling rate was increased to 11 m around termination I (313 to 511 m) and from 1500 to 3100 m depth. Thin sections were measured using the AITA developed by the Australian team [38].

From the raw AITA measurements, the microstructure is first automatically determined using an image analysis procedure initially proposed by Gay et al. [42]. When two crystals have close orientations, the automatic procedure often failed to detect the corresponding grain boundary and manual corrections were made. For each grain  $k$  within the microstructure, an average  $c^k$  axis is calculated over all the pixels within the considered grain [40]. Thus the texture is completely defined: the  $c$  axis orientations as well as topological information of the microstructure (grain size, neighbouring relation between grains...) are both specified. An example of a texture sampled at 1767.8 m depth is presented in Figure 2.

### 3.2 Parameters describing the texture

All the parameters used in this work to characterize the ice polycrystal have been detailed by Durand et al. [40] or [32] and are briefly recalled below.

#### 3.2.1 Mean crystal size

The mean grain (crystal) size is estimated through the use of the mean grain radius:

$$\langle R \rangle = \frac{1}{N_g} \sum_{k=1}^{N_g} A_k^{1/2} \quad (3)$$

where  $A_k$  is the cross-sectional area in  $\text{mm}^2$  of the grain  $k$  and  $N_g$  is the number of non-intersecting grains within the microstructure. This definition is consistent with previous work made on the microstructure of EDC (see section 3.3).  $1\sigma$  confidence intervals on  $\langle R \rangle$  can be estimated using the relation (see Durand et al. [40] for details):

$$\sigma_{\langle R \rangle} = \left( 0.02 + 0.44 \times N_g^{-1/2} \right) \times \langle R \rangle$$

#### 3.2.2 Second order orientation tensor

As suggested by Woodcock [43], the essential features of an orientation distribution can be well characterized by the second order orientation tensor  $\mathbf{a}^{(2)}$ :

$$\mathbf{a}^{(2)} = \sum_{k=1}^{N_g} f_k \mathbf{c}^k \otimes \mathbf{c}^k \quad (4)$$

where  $f_k = A_k^{3/2} / \sum_{j=1}^{N_g} A_j^{3/2}$  is the volume fraction of grain  $k$  and  $\mathbf{c}^k$  is the unit vector directed along the  $c$ -axis of the grain  $k$ . In previous studies, equal-weighted grains were usually used to calculate  $\mathbf{a}^{(2)}$  as  $f_k$  was set to  $1/N_g$ . Here we follow the recommendation of Gagliardini et al. [44] who showed that the volume weighted fraction gives a better description of the fabric.  $\mathbf{a}^{(2)}$  is by definition symmetric and, in the symmetry reference frame  $R^{sym}$  constructed from the three eigenvectors  $\mathbf{e}_i$  ( $i = 1, 2, 3$ ),  $\mathbf{a}^{(2)}$  is obviously diagonal. In  $R^{sym}$ , the length of the axis in direction  $\mathbf{e}_i$  ( $i = 1, 2, 3$ ) of the ellipsoid that best fits the density distribution of the grain orientations is proportional to the corresponding eigenvalues  $a_i^{(2)}$ . As examples, an isotropic fabric implies  $a_1^{(2)} = a_2^{(2)} = a_3^{(2)} = 1/3$  whereas a single maximum implies  $a_1^{(2)} > a_2^{(2)} \simeq a_3^{(2)}$ . Note that the eigenvalues verify  $a_1^{(2)} + a_2^{(2)} + a_3^{(2)} = 1$  by definition and we assume that  $a_1^{(2)} > a_2^{(2)} > a_3^{(2)}$  in what follows. As well as the mean grain size, error bars, closely related to the number of grains within the texture, can be defined. Whatever the considered eigenvalue  $a_i^{(2)}$ , its standard deviation is defined by (see Durand et al. [40] for details):

$$\sigma_{a_i} = \left( -1.64 \times (a_1^{(2)})^2 + 1.86 \times a_1^{(2)} - 0.14 \right) \times N_g^{-1/2}$$

As mentioned in the introduction,  $c$  axes cluster toward the compressional axis which is supposed to correspond to the in-situ vertical direction. Therefore the angle  $\phi$  between  $\mathbf{e}_1$  and the in situ vertical can be a highlighting parameter that is simply given by:

$$\phi = \arccos(\mathbf{e}_1 \cdot \mathbf{e}_z) \in [0, \frac{\pi}{2}] \quad (5)$$

where  $\mathbf{e}_z$  corresponds to the in-situ vertical.

#### 3.2.3 Relationship between neighbouring crystals

As shown by Alley et al. [30], the study of the misorientation angle between neighbouring grains can provide information on the occurrence of *rotation recrystallization*. Thanks to a stricter definition of grain boundaries (GB), Durand et al. [32] have recently proposed a new method to investigate the relationship between neighbouring grains and applied their method to the upper 1000 m of the *NorthGRIP* ice core. The procedure is briefly recalled here. First, for each grain boundary defined by the limit between two neighbouring grains  $i$  and  $j$ , the angle  $\psi_{ij}$  defined by the two  $c$ -axes  $\mathbf{c}^i$  and  $\mathbf{c}^j$  as well as the relative length  $l_{ij}$  of the considered GB (with respect to the total length of GBs within the sample) are calculated. Then, the distribution  $D_{correl}$  of the relative length  $l_{ij}$  as a function of the misorientation angle is computed. Secondly, for each grain within the microstructure, a new orientation chosen among the orientations present in the fabric is randomly assigned: the fabric is reshuffled ( $\psi_{ij}$  is modified) without altering the microstructure ( $l_{ij}$  is not affected). A distribution of  $l_{ij}$  vs  $\psi_{ij}$  can be calculated for this uncorrelated texture. This procedure is

repeated 200 times leading to the estimation of an average distribution and a  $1\sigma$  spread of uncorrelated textures. This allows us to define a  $3\sigma$  envelope which would contain  $D_{correl}$  for low angle grain boundaries ( $\psi_{ij} < 10^\circ$ ) if no rotation recrystallization was affecting misorientation angles between neighbouring grains. Application of this method on EDC samples is presented in Section 4.2.

### 3.3 Previous studies of the microstructure and fabric evolutions along EDC

Most of the existing crystallographic studies of the EDC core have been shared between microstructure and fabric studies. In this section we briefly recall the main results already obtained. In the light of the new measurements of the whole texture presented in this work and detailed in Section 3.4, some of the previous works are further discussed in Section 4.

#### 3.3.1 Microstructure evolution

The evolution of the microstructure along the EDC core has been intensively studied during the past years. Firstly, Gay et al. [42] presented an automatic image analysis procedure enabling the reconstruction of the microstructure and applied this method to the upper 360 meters of the EDC core. In this part of the core, that corresponds to the Holocene period, the average grain size steadily increases with depth. This is due to the normal grain growth process that is driven by a reduction of the total grain boundary energy and the grain growth law exponent  $m$  was estimated to 3.2 [12]. Weiss et al. [45] inspected the evolution of the mean grain radius  $\langle R \rangle$  down to 580 m depth, pointing out a sharp decrease of  $\langle R \rangle$  linked with the Holocene-Last Glacial Maximum transition (Termination I). The impact of impurities was discussed, and a predominant role of dust particles through a pinning mechanism, was considered. Indeed, Weiss et al. [45] demonstrated that  $R_z$  is quantitatively in agreement with  $\langle R \rangle$  during the Last Glacial Maximum (LGM) if the particles are preferentially located along grain boundaries. This hypothesis has been experimentally validated through X-Ray tomography on ice sampled in LGM ice along EDC [12]. Measurements also revealed a sharp decrease of  $\langle R \rangle$  associated to termination II (around 1750 m) and a smaller grain size is also attributed to the enhancement of the pinning effect of dust particles during stage 6. The effect of impurities on grain growth along the EDC core is discussed in detail and modeled down to 2135 m by Durand et al. [12]. Finally, smaller grain size associated with glacial periods was further observed down to 3139 m depth [46].

Durand et al. [15] have developed an original method to measure a deformation tensor from the microstructure and apply this method to EDC down to 3000 m. They show that: (i) although the flow at a dome is assumed to be axisymmetric and ice layer thinning is supposed to result from vertical compression only, horizontal shear is present already well above the basal part of the ice sheet, and (ii) in contradiction with current assumptions of ice

flow models, the vertical strain rate is not always negative.

#### 3.3.2 Fabric evolution

Wang et al. [41] described the evolution of the fabric from 81 m to 1451 m depth, showing a strengthening of the fabric with increasing depth: from a close to random distribution of  $c$  axes at 81 m, the fabric evolves progressively to a vertical single maximum at greater depths. Such a fabric evolution characterizes uniaxial compression, the main deformation process below a dome. Moreover, the EDC fabric evolution is in good agreement with the fabric evolutions observed along the Dome F and GRIP cores, supporting the common assumption that the fabric strength in the upper part of ice sheets depends mainly on the cumulative strain.

Recent work [47] investigated the evolution of the fabric from 1500 m down to 2000 m depth. During Termination II (around 1750 m), a sharp and unexpected strengthening of the fabric is observed. Such clustering has already been observed for cores drilled on ice-sheet flanks, and it was attributed to horizontal shear enhancement in ice deposited during glacial periods. This result strongly suggests that horizontal shear occurs in the vicinity of EDC. This work was based on both fabric and microstructure measurements and main conclusions will be recalled in the following discussion (see Section 4.3.1).

### 3.4 Results and comparison with existing studies

Here we compare the new results with those previously obtained. All the parameters adapted from previous studies have a subscript which refers to the first author of the original publication.

Figure 3 shows the evolution of the dust content down to 3128 m (a), together with the evolution of  $\langle R \rangle_{EPICA}$  (b) as they were presented in EPICA community [46]. The  $\langle R \rangle$  values obtained in this study are plotted together with their  $1\sigma$  error bars in Figure 3c and they are in excellent agreement with the previous results. Indeed, the new measurements above 2500 m are included in the envelope defined by  $\langle R \rangle_{EPICA} \pm 3\sigma$ . For the deepest part of the core, the variability in the grain size from sample to sample is more important which makes the comparison between the two data sets more difficult. However, the large variations of  $\langle R \rangle$  and  $\langle R \rangle_{EPICA}$  are consistent with respect to their depth ranges and amplitudes. As a general trend, the average grain size increases with depth (and so age) from 0.9 mm at 101 m to 9.4 mm at 3133 m. Because (i) the sample size is constant and (ii)  $\langle R \rangle$  increases with depth, the number of grains in each sample  $N_g$  decreases, and then statistical significance of the measurements also decreases with depth. This effect becomes important in the very bottom part of the core where we observe only very few grains in each sample. Furthermore, the increase of  $\langle R \rangle$  is punctuated by significant local decreases and it can be easily seen from Figure 3 that samples presenting smaller  $\langle R \rangle$  are observed during

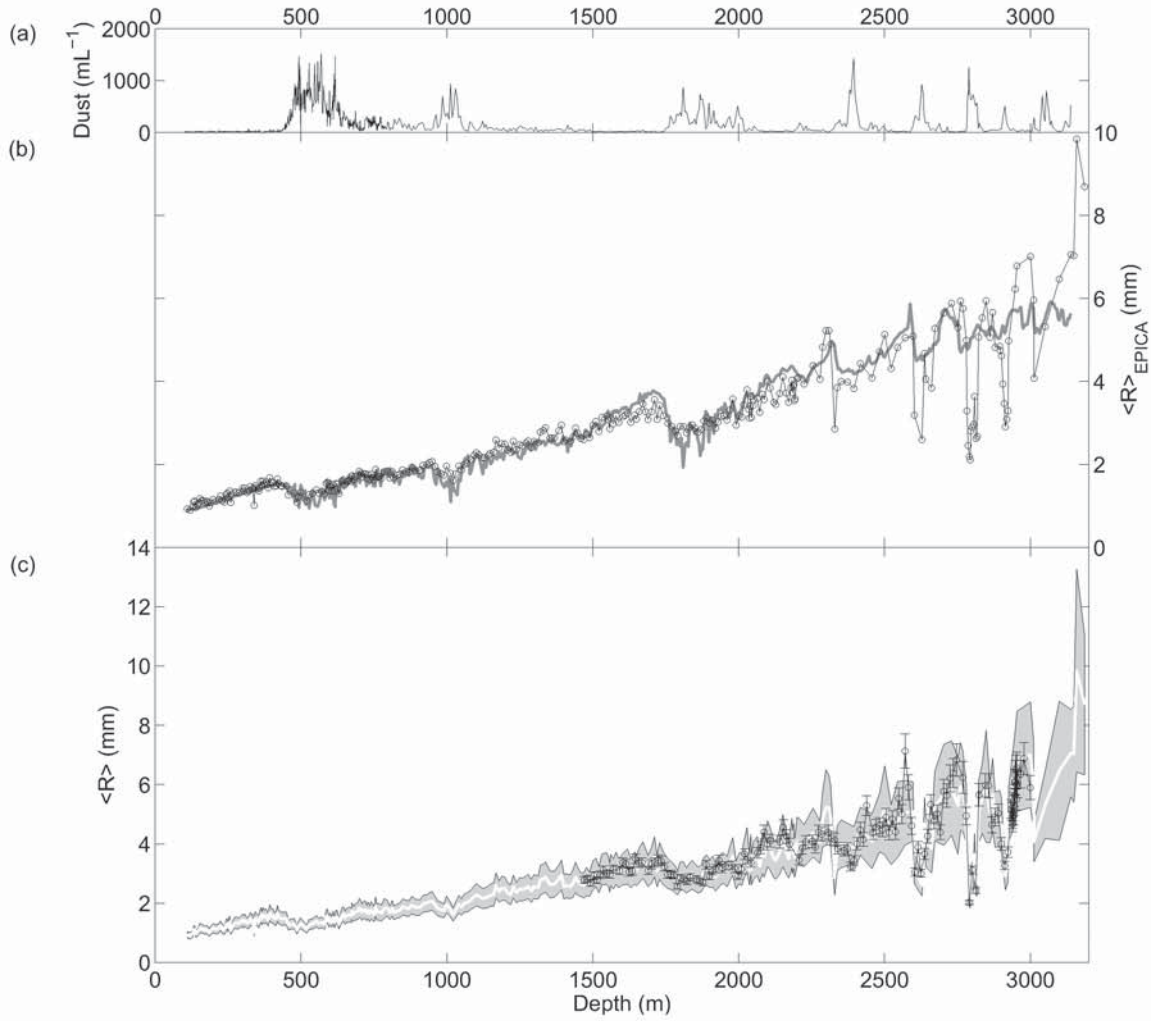


Figure 3: (a) Evolution of the dust content versus depth [46]. (b) Evolution of the mean grain radius  $\langle R \rangle_{EPICA}$  as presented in the EPICA community [46] (black open symbols). Continuous gray line corresponds to the model output (see Section 3.4). (c) Evolution of  $\langle R \rangle$  estimated from the new measurements with error bars corresponding to  $\pm 1\sigma$  confidence interval. White thick line shows  $\langle R \rangle_{EPICA}$  and grey area gives the  $\langle R \rangle_{EPICA} \pm 3\sigma$  confidence interval.

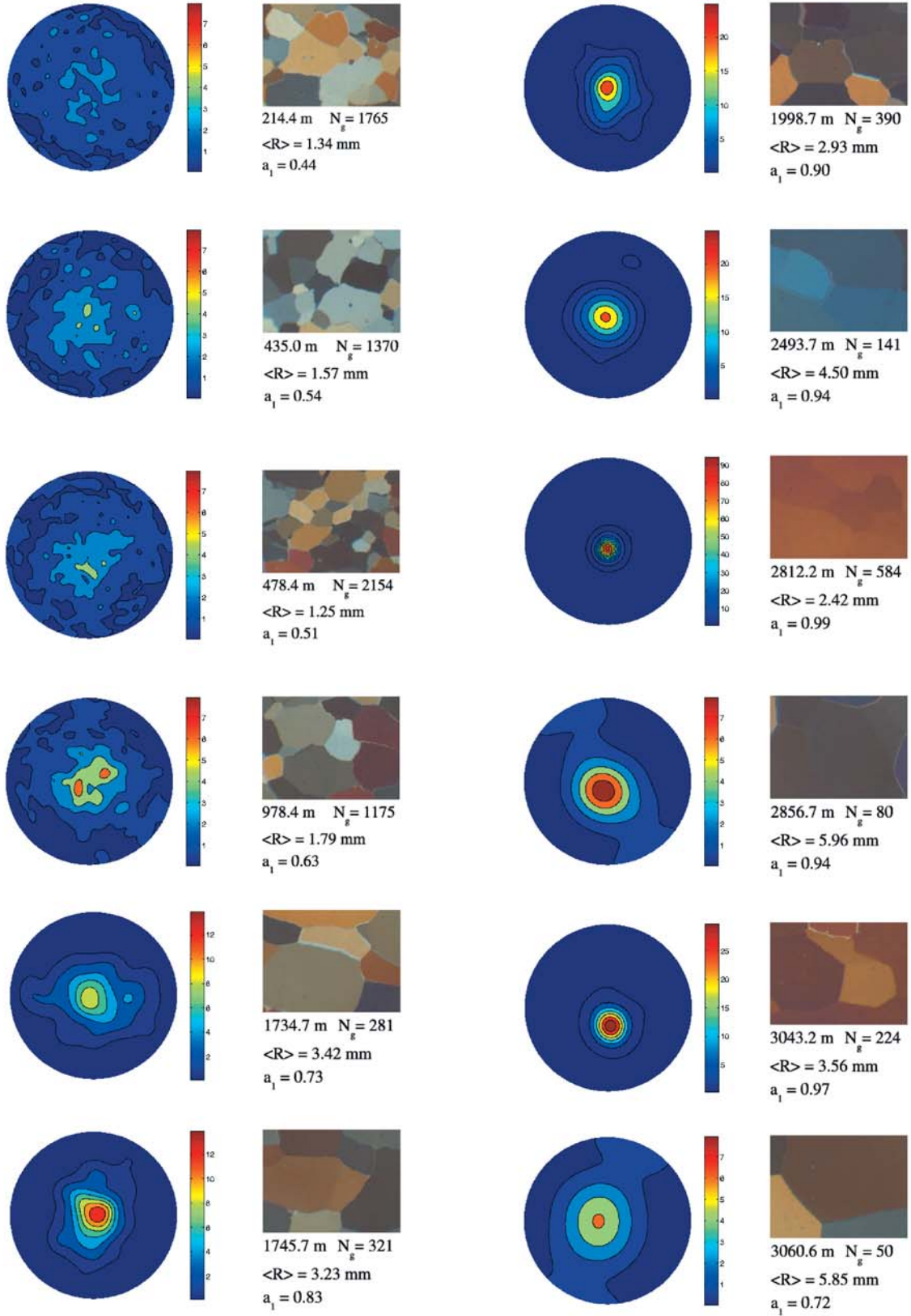


Figure 4: Fabric diagrams and details of thin-section photographs. Depth, number of grains  $N_g$ , mean grain radius  $\langle R \rangle$  and first eigenvalues of the second order orientation tensor  $a_1^{(2)}$  are indicated below the thin section images. For the fabric diagrams, the value detailed by the color scale gives the observed orientation density relative to isotropic orientation density. Note that the color scale is adjusted for each diagram.

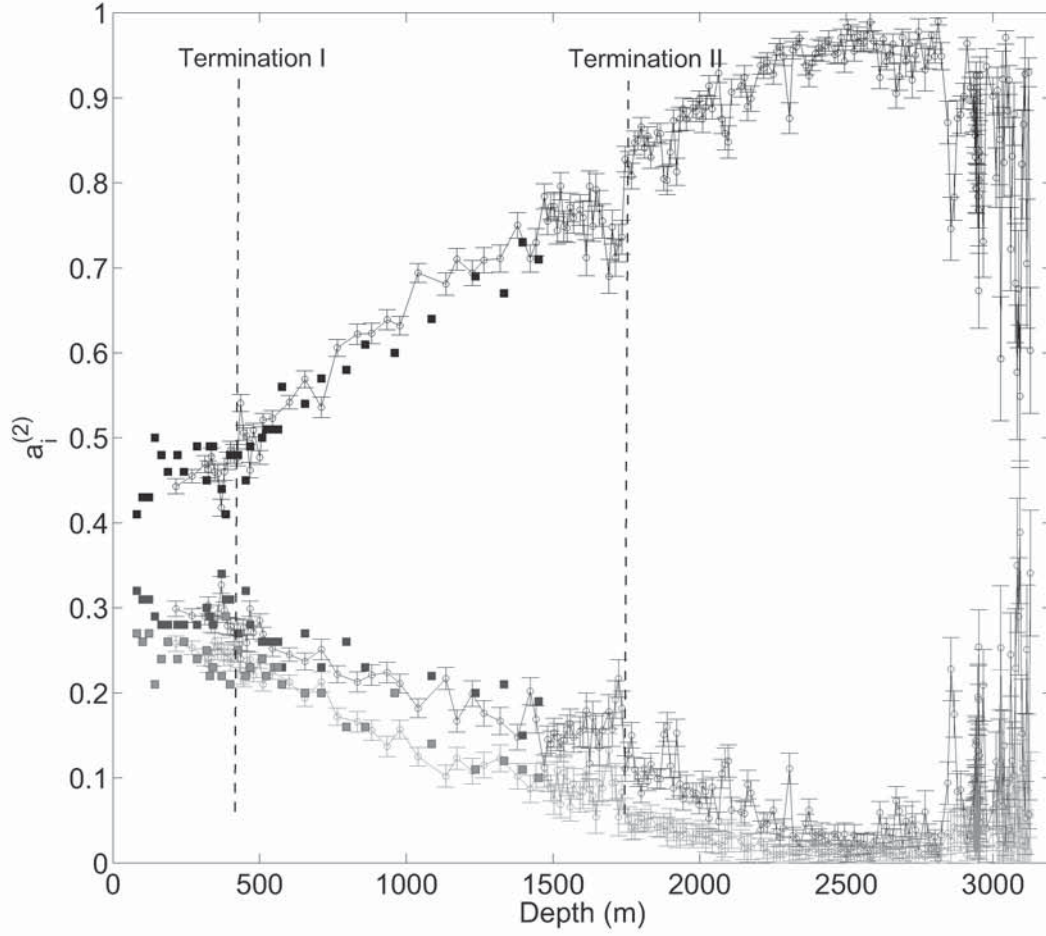


Figure 5: Eigenvalues of the second order orientation tensor versus depth. Open symbols corresponds to the measurements recently done,  $a_1^{(2)}$  is in black,  $a_2^{(2)}$  in dark grey and  $a_3^{(2)}$  in light grey. Error bars correspond to  $1\sigma$  confidence level. Previous measurements made by Wang et al. [41] are presented with filled squares (same color code). Vertical dotted lines point out Termination I and II.

periods with high dust content. The reasons of such an evolution of  $\langle R \rangle$  are discussed in Section 4.1.

Figure 4 shows some of the fabric distributions as well as detail of an image of each thin section. Rather than the classical point plots, we have chosen to present the fabric distribution using contour plots on an equal area mesh. This representation gives a better description of the fabric for small or very large populations of grains. Note that all the contour-plots are presented in a horizontal reference frame, *i.e.*, the in situ vertical (the core axis) is at the centre of the polar plot. As a general trend, one can see that a vertical single maximum is forming with increasing depth even if large fluctuation of the clustering can be observed below 2800 m.

The overall evolution of the fabric can be well described by the evolution of the second order orientation tensor. Figure 5 shows the evolution of  $a_i^{(2)}$  with  $1\sigma$  error bars. Previous measurements made by Wang et al. [41] are also shown in Figure 5 (filled squares) and are well in agreement with the present results. The fabric starts from a quasi random state at 81 m:  $a_{1Wang}^{(2)} \simeq 0.41$ ,  $a_{2Wang}^{(2)} \simeq 0.32$  and  $a_{3Wang}^{(2)} \simeq 0.27$  and, as a general feature, it evolves to a vertical single maximum with  $a_1^{(2)}$  reaching 0.99 whereas  $a_2^{(2)} \simeq a_3^{(2)} \simeq 0.005$  at 2813 m. Two particular aspects can be noted: (i) as already mentioned, there is a sharp and significant increase of  $a_1^{(2)}$  around 1750 m and this increase is concurrent with the grain size decrease observed at the climatic termination II (see Figure 3). Note also a significant decrease of  $a_1^{(2)}$  in an approximatively 60 m thick layer located just above termination II (MIS 5.5). (ii) Below 2800 m the clustering of the fabric is less pronounced compared to the above layers while the variability of  $a_1^{(2)}$  is very pronounced. A discussion of the fabric evolution is given in Section 4.3.

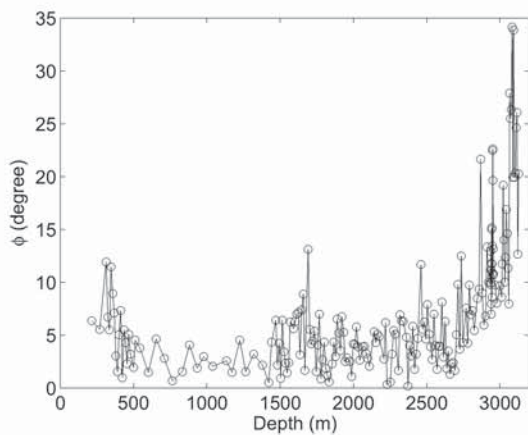


Figure 6: Evolution of  $\phi$  versus depth.

The angle  $\phi$  between the in situ vertical and  $e_1$  is shown on Figure 6.  $\phi$  remains constant around  $5^\circ$  down to 2700 m depth from where it increases up to  $35^\circ$  below 3000 m. Uncertainties in the estimation of  $\phi$  come mainly from the orientation of the ice sample with re-

spect to the core axis as well as the orientation of the thin section during the measurement. Such uncertainties are difficult to quantify, but we believe that the accuracy of  $\phi$  is better than  $10^\circ$ . Because a perfect random fabric has an infinite number of symmetry axes, the calculation of  $e_1$  can fluctuate from sample to sample in the upper part of the core where the clustering of the fabric is weak. This certainly explains the slightly elevated values of  $\phi$  above 500 m. The value of  $\phi$  has to be compared with the inclination of the borehole, which remains constant below  $1^\circ$  down to 2700 m before it increases to a maximum of  $5^\circ$  around 3000 m. Despite those uncertainties, the high values observed for the very bottom part are definitively significant.

## 4 Discussion

### 4.1 Grain size evolution

As mentioned previously, the general increase of  $\langle R \rangle$  is punctuated by sharp decreases in relation with climatic terminations. The identification of the dominant mechanism at the origin of these decreases has been discussed for a long time. As a contribution of this 20 years long debate, Durand et al. [12] proposed a numerical model of the evolution of  $\langle R \rangle$  in deep ice cores that takes into account (i) recrystallization processes (normal grain growth and rotation recrystallization) and (ii) the pinning effect induced by dust particles, bubbles and clathrates on grain boundaries. The model was run down to 2135 m and was able to reproduce accurately the variations of  $\langle R \rangle$  down to 1750 m. Below this depth, the model predicts too small grain size during high dust content events, *i.e.* the pinning effect of dust particles is too strong. A thermally activated unpinning of grain boundaries from dust particles has now been introduced following the work of Gore et al. [48] on ferrous alloys. Including this unpinning process, the model correctly reproduces the evolution of  $\langle R \rangle$  down to 2135 m, *i.e.* the whole grain size profile at the time of the study. Figure 3b shows the result of the model which has been extended down to 3139 m (thick grey line) using the same conditions as Durand et al. [12]. Although the general increase of  $\langle R \rangle$  is well reproduced, two aspects have to be discussed.

(i) The amplitudes of the decreases during the climatic terminations are not well reproduced by the model below 2200 m. Due to the implementation of the unpinning effect in the model, the proportion of dust particles located along grain boundaries decreases rapidly below 1000 m and falls to almost 0 below 2000 m [12]. As a consequence, the effect of dust on grain growth is too weak to counteract grain growth during glacial periods. It is interesting to note that due to the unpinning of grain boundaries, grain boundaries can move and then could be pinned once again by dust particles. Thus, an equilibrium between pinning and unpinning could appear, which would probably lead to a higher concentration of particles along grain boundaries compared to the model prediction. It is, however, difficult to go further into the interpreta-

tion as we do not have any quantitative information on the particles location. One of the main conclusions of this modeling exercise is that dust particle location is a predominant parameter to estimate the pinning strength. In the future, a better characterization of the location of impurities in the ice is needed to understand in more details the grain size evolution in ice cores.

(ii) Below 2900 m,  $\langle R \rangle$  is larger than the prediction of the model during interglacial periods and this discrepancy increases with depth. As the temperature is close to  $-10^\circ\text{C}$  at 2900 m and increases towards  $-5^\circ\text{C}$  at 3130 m, migration recrystallization could occur within this depth range. Moreover, the migration rate of grain boundaries is several orders of magnitude larger for migration recrystallization compared to normal grain growth for a given temperature [34]. Therefore, the underestimation of the model could be attributed to the onset of migration recrystallization, as this process is not taken into account in the model.

#### 4.2 Low angle grain boundaries and rotation recrystallization

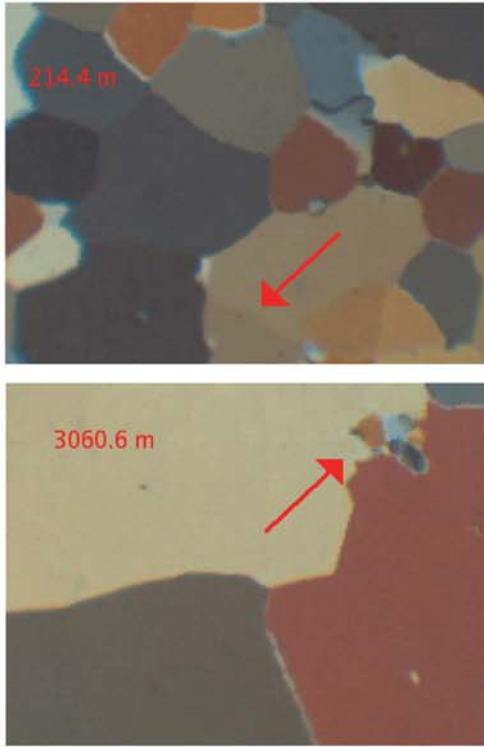


Figure 7: Upper picture: detail of a thin-section sampled at 214.4 m, the arrow pointed out a subgrain boundary (see section 4.2 for details). Lower picture: details of a thin-section sampled at 3060.6 m, the arrow pointed out small 2-sides grains (see section 4.3.2 for details).

Some low angle grain boundaries can be observed in the upper part of the ice core as pointed out by an arrow on the photography of the thin section taken at 214.4 m (see Figure 7). We used the method developed by Durand et al. [32] and briefly recalled in Section 3.2.3 to test

the significance of the correlation between neighbouring grains. Figure 8 shows the  $D_{\text{correl}}$  distribution (thick black line) for a texture sampled at 214.4 m together with 1, 2 and  $3\sigma$  envelopes calculated from 200 reshuffled textures (gray tones). Low angle GBs ( $\psi_{ij} < 10^\circ$ ) are significantly overestimated compared to the reshuffled textures. Similar results have been obtained for all the shallowest samples. This suggests that *rotation recrystallization* is already occurring in the upper part of the ice sheet.

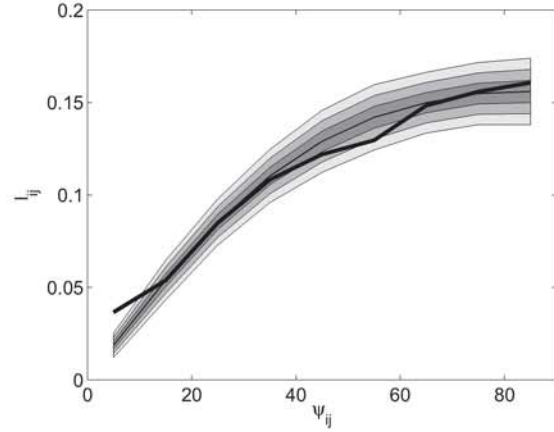


Figure 8: Distribution of the relative length of GBs as a function of the misorientation angle  $\psi_{ij}$  for the texture sampled at 214.4 m.  $D_{\text{correl}}$  is plotted with a dark solid line, whereas gray tones corresponds to 1, 2 and  $3\sigma$  deviations estimated from 200 reshuffled textures. The distribution and its envelope are calculated for  $10^\circ$  bins.

Further, the impact of *rotation recrystallization* can be estimated by looking at the evolution of the relative population of subgrains  $P_{0 < \psi_{ij} < 10^\circ}$ .  $P_{0 < \psi_{ij} < 10^\circ}$  is plotted versus the cumulative strain  $\varepsilon_{zz}$  on Figure 9 (filled circles).  $\varepsilon_{zz}$  is estimated through the 1D flow model used to determine the evolution of age along the core [49]. Standard deviation has been estimated for each sample by repeating 200 times a reshuffling of the fabric (see section 3.2.3 or Durand et al. [32] for details). Except for one sample,  $P_{0 < \psi_{ij} < 10^\circ}$  is significantly over-estimated compared to reshuffled experiments.  $P_{0 < \psi_{ij} < 10^\circ}$  increases linearly from 3 to 6% from  $\varepsilon_{zz} = -0.07$  to  $\varepsilon_{zz} = -0.36$  (respectively 269.4 and 1039.95 m) with a regression coefficient of 0.90. A similar linear increase of  $P_{0 < \psi_{ij} < 10^\circ}$  has been observed along *NorthGRIP* (empty circles) [32]. However, the slope of the linear regression is almost 2 times larger in the *NorthGRIP* case ( $-0.10$  and  $-0.19$  respectively). We believe that this slope is a function of the grain growth rate  $K$  (see Equation 1) and the strain rate  $\dot{\varepsilon}$ , as  $K$  controls the rate of grain boundary consumption (normal grain growth) and  $\dot{\varepsilon}$  controls the dislocation production and then the rate of new low-angle grain boundary production (rotation recrystallisation) (see also [50]). Then, Figure 9 confirms that *rotation recrystallization* is more effective (relative to *normal grain growth*) along *NorthGRIP* than along EDC. This is in agreement with the steady grain size observed along *NorthGRIP* [31].

This linear increase also seems to indicate that the fragmentation rate of grains is constant through the strain. However, it is difficult to estimate quantitatively the relative impact of these two processes on  $P_{0 < \psi_{ij} < 10}$ . Simulation with an explicite microstructure evolution model would be required to enlight this point [51].

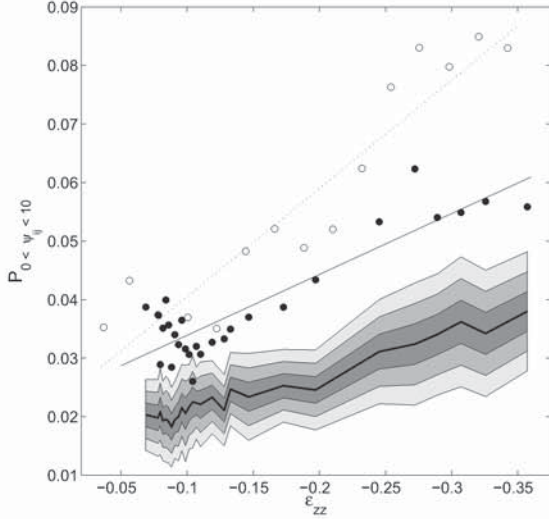


Figure 9: Evolution of  $P_{0 < \psi_{ij} < 10}$  versus  $\epsilon_{zz}$  for the EDC core (filled circles). Linear regression is plotted as a straight black line. 1, 2 and  $3\sigma$  deviations are shown with grey tones. For comparison  $P_{0 < \psi_{ij} < 10}$  measured along NorthGRIP is also shown (empty circles) with the corresponding linear regression (dotted line).

### 4.3 Fabric

As briefly discussed in Section 3.4, the fabric evolves from a roughly random fabric close to the surface into a vertical single maximum fabric at greater depths. This first order classical description of fabric evolution at a dome has, however, to be moderated in the EDC case for at least two reasons. (i) The prolongation of the trends towards the surface does not give an initially isotropic fabric. Moreover, Diprinzio et al. [52] have shown some sections with an already clustered fabric ( $a_1^{(2)} \sim 0.55$ ) at a depth of 22 m in the Siple Dome ice core. This questions our understanding of surface processes and will have to be clarified in the future. (ii) The fabric shows a slight elongation along one horizontal direction as  $a_2^{(2)}$  is significantly larger than  $a_3^{(2)}$  below 2000 m. This is, however, expected as it is consistent with the theory of the topology of ice-sheet centers [53] for a dome with a shape slightly elongated [in the North-Est direction, 54].

Besides those features, two other aspects have to be discussed in more details: the significant strengthening of fabric around 1750 m as well as the opening and large variability of fabric below 2800 m. This is the aim of the following sections.

#### 4.3.1 Fabric strengthening during termination II

A detailed discussion on the evolution of fabric between 1500 and 2000 m along EDC as well as comparisons with numerical simulations can be found in Durand et al. [47]. The main results are recalled here.

Durand et al. [47] proposed three hypothesis to explain the origin of the observed strengthening: (i) a change in the initial fabric at the time of deposition, (ii) a change in the shape of the dome and (iii) a modification in the effective viscosity of ice related to climate. (iii) appears to be the most probable explanation, but it requires significant shearing in order to initiate the positive feedback at the root of the fabric strengthening [14]. Indeed, an initial difference in shear viscosity induced by a difference in grain size or impurity content can be magnified under horizontal shear because horizontal shear strengthens the vertical single maximum fabric which then becomes easier to shear. Horizontal shear is negligible under a perfect dome, but many theoretical assertions lead to believe that this assumption may not hold for the EDC core: the divide is not inevitably co-located with the highest surface elevation and the isoline corresponding to zero shear could have a sinuous shape. Moreover, some microstructural measurements as well as echo soundings indicate the presence of shear along EDC. Such a shearing scenario allows us to correctly explain the observations through a numerical experiment. Indeed, using a local higher order anisotropic ice flow model, Durand et al. [47] have correctly reproduced the sharp strengthening between two layers presenting a difference in their viscosity. The model also reproduces the decrease of  $a_1^{(2)}$  in the upper layer, as observed on the EDC data. In terms of ice flow, numerical experiments have shown that the discontinuity of the viscosity of ice implies a discontinuity in the shear strain-rate and a discontinuity in the slope of the longitudinal strain-rate. Shear strain-rate and slope of the longitudinal strain-rate are higher in softer layers as compared to harder layers. These differences have implications on the thinning function as the slope of the thinning function is affected, but due to the continuity of the longitudinal strain-rate, there is no differential thinning between adjacent layers. It is, however, impossible with these results to help the ice core dating community as the flow conditions vary from site to site even if they present a similar glaciological context.

What about the other Terminations, do we observe a similar strengthening of the fabric there? As mentioned by Durand et al. [32], such a clustering is not observed during termination I in the data of Wang et al. [41]. It is also difficult to find such tendency in the new measurements made around Termination I and presented in Figure 5. As shear increases with depth, we believe that higher clustered layers do not have the opportunity to develop in the upper part of the core. On the other hand, below 1750 m, the clustering of the fabric is already very pronounced  $a_1^{(2)} > 0.8$  so that enhanced clustering due to shear is less visible. However, it is interesting to note that below

2800 m, where the fabric present a large variability, all the layers presenting smaller grains (glacial maxima) are much more clustered than the surrounding layers. This can be seen in Figure 4 by comparing the textures sampled at 3043.2 m (stage 16.3) and 3060.6 m (stage 17.3) respectively.

#### 4.3.2 Bottom part: is migration recrystallization occurring?

In Figure 10 we present the evolution of  $a_i^{(2)}$  for the deepest part of the EDC core compared with that of GRIP within a similar depth range (below 2500 m) [21]. The two records look very similar although the low resolution of the GRIP record does not allow for a strict comparison. According to Thorsteinsson et al. [21] the decrease in  $a_1^{(2)}$  observed for the deepest part of the GRIP core, is attributed to the occurrence of migration recrystallization. However, the authors acknowledge that the evidence for migration recrystallization is not obvious: (i) large interlocking grains are not always observed and (ii) fabrics do not present a girdle type at  $30^\circ$  from the compressional axis as demonstrated by laboratory tests. Can a similar (or more conclusive) explanation be given to explain the fabric evolution for the last hundred meters of the EDC core? This is of primary importance. Indeed, flow disturbances that affect the duration of events below 2800 m have been detected and dating corrections have been suggested [55]. However, a clear interpretation of the physical processes at the origin of these disturbances has not been provided. If migration recrystallization is not occurring, the study of the fabric could give valuable indications on past deformation.

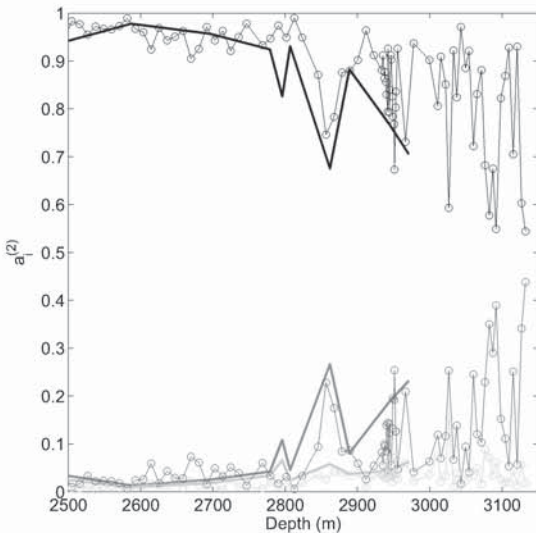


Figure 10: Eigenvalues of the second order orientation tensor versus depth.  $a_1^{(2)}$  is in black,  $a_2^{(2)}$  in dark grey and  $a_3^{(2)}$  in light grey. Open symbols along the EDC core and thick line along the GRIP core.

As mentioned in Section 2.2.3, migration recrystallization is believed to take place for temperature close to the melting point (roughly above  $-10^\circ\text{C}$ ). Since the temperature has reached  $-13^\circ\text{C}$  at 2800 m and increases to  $-2^\circ\text{C}$  at 3250 m the ice is probably warm enough for migration recrystallization to occur.

It has to be noted that the evolution of  $a_i^{(2)}$  is highly fluctuating. Indeed, the sampling rate has been increased up to 0.5 m during the transition from stage 14 to stage 15 (2933 to 2955 m), and the frequency of the clustering fluctuations increased as well: there are highly contrasting fabrics from one sample to the next. Moreover, there is no clear correlation between the fabric fluctuations and climate or chemical components. For example, between 2951 and 2956 m (stage 15),  $a_1^{(2)}$  increases from 0.67 to 0.93 although isotopic values are stable and the impurity content is relatively low and constant. The only feature that can be noticed is that layers with high impurity content and thus small mean grain size always present a strong single maximum fabric.

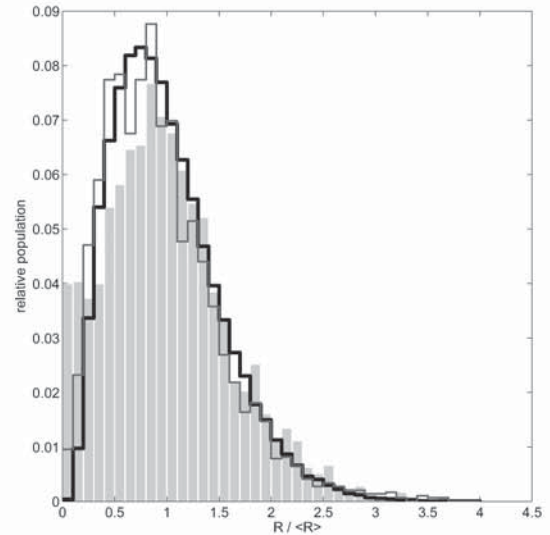


Figure 11: Normalized grain size distributions, cumulated for all the textures sampled above 2812 m (thick black lines), cumulated for textures sampled below 2812 m and presenting  $a_1^{(2)} > 0.9$  (dark gray line), cumulated for textures sampled below 2812 m and presenting  $a_1^{(2)} \leq 0.9$  (light gray area).

From 2846 m depth and downwards very small grains ( $< 1$  mm) start to appear in between the larger grains. The small grains are too small to obtain good measurements of their c-axis orientation. An illustration of such grains is presented on Figure 7 for the texture sampled at 3060.6 m. These grains are generally 2-sides (surrounded by only 2 neighbours), which is unusual as such grains would normally be rapidly consumed by normal grain growth. Consequently, these grains have probably been recently nucleated. Under normal grain growth, the normalized grain size distribution remains unaffected [29].

Then, it is reasonable to stack the normalized grain size distributions from sample to sample (at least for the upper part of the core). This allows us to improve the representation of the distribution when dealing with a low population of grains in each sample. Figure 11 is the normalized distribution stacked for all the textures sampled above 2812 m (thick black line). A distribution with a maximum followed by an exponential decaying tail is found, which is typical of a normal grain growth regime. Below 2812 m, the stack is done for textures presenting  $a_1^{(2)} > 0.9$  on one hand (dark gray line), and for  $a_1^{(2)} \leq 0.9$  on the other hand (light gray area). Textures with highly clustered fabrics ( $a_1^{(2)} > 0.9$ ) show a stacked normalized distribution very similar to the one obtained for the upper samples. On the other hand, the samples where the fabric is drastically affected ( $a_1^{(2)} \leq 0.9$ ) show a clear overestimation of smaller grains compared to the other distributions. This demonstrates that there is a clear link between the presence of small grains and the observed opening of the fabric. The first step of migration recrystallization appears to be reached (nucleation of grains). However, we have never observed the typical girdle fabric that is classically assigned to a recrystallized sample under vertical compression. Moreover, large, interlocking crystals have not been observed. This questions the effect of migration recrystallization on textures and would need to be clarified in the future.

## 5 Conclusion

New measurements of the texture (microstructure and fabric) have been done along the EDC core, from 214 m down to 3133 m depth. A review of the existing EDC texture works is given together with a discussion of the new observations.

The mean grain size steadily increases due to normal grain growth. This increase is punctuated by sharp decreases in phase with deglaciations. The dust content is much larger during glacial periods, and the larger number of dust particles during these periods induces a decrease of the grain growth rate through a pinning effect. However, the strength of this pinning effect is drastically affected by the location of particles within the ice crystals, and this effect is strong enough to quantitatively explain our observations at the condition where dust particles are preferentially located at the grain boundaries. However, this preferential location probably evolves with depth through an unpinning effect, and thus its effect on grain growth also. A better understanding of the state of impurities (solute or particle) and their location within the polycrystal would be essential to improve our knowledge on grain growth in polar ice.

As it has been observed for other cores located at a dome, fabric evolves from a quasi-random distribution at the firn-ice transition to a strong vertical single maximum with increasing depth. However, this general trend is punctuated by a sharp clustering of the fabric during

termination II (around 1750 m). The most likely explanation is that shear is not negligible along the EDC core. A difference of viscosity between layers of different periods, probably due to difference in grain size and/or in impurity content, could be the cause of a slight clustering of the fabric. A positive feedback is initiated as more clustered fabrics become easier to shear, which in turn enhance the clustering. Such clustering is not observed during termination I probably because the shearing is too weak in the upper part of the core to initiate the positive feedback. Deeper, the fabric is too clustered to observe such a variation during the following terminations. Finally, below 2846 m, the evolution of the fabric is extremely variable. As the temperature is high enough, migration recrystallization may occur. However, despite the fact that small nucleate grains appear, other fingerprints of the migration recrystallization are not obvious. This shows the limitations of our knowledge on the effect of such process on the ice polycrystal. This will have to be further investigated in the future.

## Acknowledgements

This work is a contribution to the 'European Project for Ice Coring in Antarctica' (EPICA), a joint ESF (European Science Foundation)/EC scientific programme, funded by the European Commission under the Environment and Climate Program contract ENV4-CT95-0074 and by national contributions from Belgium, Denmark, France, Germany, Italy, the Netherlands, Norway, Sweden, Switzerland and the United Kingdom. The authors wish to thank Prof. T. H. Jacka for his fruitful comments.

## References

- [1] J. M. Barnola, D. Raynaud, Y. S. Korotkevich, and C. Lorius. Vostok ice core provides 160000-year record of atmospheric  $\text{CO}_2$ . *Nature*, 329:408–414, 1987.
- [2] J. Jouzel et al. Orbital and millennial Antarctic climate variability over the past 800000 years. *Science*, 317:793–796, 2007.
- [3] S. O. Rasmussen, K. K. Andersen, A. M. Svensson, J. P. Steffensen and B. M. Vinther, H. B. Clausen, M.-L. Siggaard-Andersen, S. J. Johnsen, L. B. Larsen, D. Dahl-Jensen, M. Bigler, R. R. H. Fischer, K. Goto-Azuma, M. E. Hansson, , and U. Ruth. A new greenland ice core chronology for the last glacial termination. *Journal of Geophysical Research*, 111(D06102), 2006.
- [4] D. Dahl-Jensen, T. Thorsteinsson, R. Alley, and H. Shoji. Flow properties of the ice from the Greenland Ice Core Project ice core: the reason for folds? *J. Geophys. Res.*, 102(C12):26831–26840, 1997.
- [5] R. B. Alley, A. J. Gow, D. A. Meese, J. J. Fitzpatrick, E. D. Waddington, and J. F. Bolzan. Grain-

- scale processes, folding, and stratigraphic disturbance in the GISP2 ice core. *J. Geophys. Res.*, 102(C12):26819–26830, 1997.
- [6] D. Raynaud, J.-M. Barnola, R. Souchez, R. Lorrain, J.-R. Petit, P. Duval, and V. Y. Lipenkov. CO<sub>2</sub> and climate: the case of Marine Isotopic Stage (MIS) 11. *Nature*, 436:39–40, 2005.
- [7] P. Duval, M. F. Ashby, and I. Anderman. Rate controlling processes in the creep of polycrystalline ice. *J. Phys. Chem.*, 87:4066–4074, 1983.
- [8] N. Azuma and A. Higashi. Formation processes of ice fabric pattern in ice sheets. *Ann. Glaciol.*, 6:130–134, 1985.
- [9] C. J. Van der Veen and I. M. Whillans. Development of fabric in ice. *Cold Reg. Sci. Technol.*, 22(2):171–195, 1994.
- [10] F. Gillet-Chaulet, O. Gagliardini, J. Meyssonier, T. Zwinger, and J. Ruokolainen. Flow-induced anisotropy in polar ice and related ice-sheet flow modelling. *J. Non-Newtonian Fluid Mech.*, 134(1-3):33–43, 2006.
- [11] R. B. Alley, J. H. Perepezko, and C. R. Bentley. Grain growth in polar ice: II. application. *J. Glaciol.*, 32(112):425–433, 1986b.
- [12] G. Durand, J. Weiss, V. Lipenkov, J. M. Barnola, G. Krinner, F. Parrenin, B. Delmonte, C. Ritz, P. Duval, R. Roethlisberger, and M. Bigler. Effect of impurities on grain growth in cold ice sheets. *J. Geophys. Res.*, 111(F01015), 2006.
- [13] K. M. Cuffey, T. Thorsteinsson, and E. D. Waddington. A renewed argument for crystal size control of ice sheet strain rates. *J. Geophys. Res.*, 105(B12):27889–27894, 2000.
- [14] W. S. B. Paterson. Why ice-age is sometimes soft. *Cold. Reg. Sci. Technol.*, 20(1):75–98, 1991.
- [15] G. Durand, F. Graner, and J. Weiss. Deformation of grain boundaries in polar ice. *Eur. Phys. Lett.*, 67(6):1038–1044, 2004.
- [16] R. B. Alley. Flow-law hypotheses for ice-sheet modeling. *J. Glaciol.*, 38(129):245–256, 1992.
- [17] J. E. Burke and D. Turnbull. Recrystallization and grain growth. *Progress in Metal Physics*, 3:220–292, 1952.
- [18] M. Hillert. On the theory of normal and abnormal grain growth. *Acta Met.*, 13:227–238, 1965.
- [19] M. P. Anderson, G. S. Grest, and D. J. Srolovitz. Computer simulation of normal grain growth in three dimensions. *Philos. Mag. B.*, 59(3):293–329, 1989.
- [20] D. Weygand, Y. Bréchet, J. Lépinoux, and W. Gust. Three dimensionnal grain growth: a vertex dynamics simulation. *Phil. Mag. B.*, 79(5):703–716, 1998.
- [21] T. Thorsteinsson, J. Kipfstuhl, and H. Miller. Textures and fabrics in the GRIP project. *J. Geophys. Res.*, 102(C12):26583–26599, 1997.
- [22] V. Ya. Lipenkov, N. I. Barov, P. Duval, and P. Pimienta. Crystalline texture of the 2083m ice core at Vostok station, antarctica. *J. Glaciol.*, 35(121):392–398, 1989.
- [23] R. B. Alley, J. H. Perepezko, and C. R. Bentley. Grain growth in polar ice: I. theory. *J. Glaciol.*, 32(112):415–424, 1986a.
- [24] D. A. Fisher and R. M. Koerner. On the special rheological properties of ancient microparticle-laden northern hemisphere ice as derived from bore-hole and core measurements. *J. Glaciol.*, 32(112):501–510, 1986.
- [25] J. R. Petit, P. Duval, and C. Lorius. Long-term climatic changes indicated by crystal growth in polar ice. *Nature*, 326:62–64, 1987.
- [26] R. B. Alley and G. A. Woods. Impurity influence on normal grain growth in the GISP2 ice core, Greenland. *J. Glaciol.*, 42(141):1996, 1996.
- [27] A. J. Gow, D. A. Meese, R. B. Alley, J. J. Fitzpatrick, S. Anandakrishnan, G. A. Woods, and B. C. Elder. Physical and structural properties of the Greenland Ice Sheet Project 2 ice core: a review. *J. Geophys. Res.*, 102(C12):26559–26575, 1997.
- [28] J. Li, T. H. Jacka, and V. Morgan. Crystal-size microparticle record in the ice core from Dome Summit South, Law Dome, East Antarctica. *Ann. Glaciol.*, 27:343–348, 1998.
- [29] F. J. Humphreys and M. Hatherly. *Recrystallization and related annealing phenomena*. Pergamon-Elsevier Science Ltd, 1996.
- [30] R. B. Alley, A. J. Gow, and D. A. Meese. Mapping c-axis fabrics to study physical processes in ice. *J. Glaciol.*, 41(137):1995, 1995.
- [31] A. Svensson, K. G. Schmidt, D. Dahl-Jensen, S. J. Johnsen, Y. Wang, J. Kipfstuhl, and T. Thorsteinsson. Properties of ice crystals in NorthGRIP late-to middle- Holocene ice. *Ann. Glaciol.*, 37:113–118, 2003.
- [32] G. Durand, D. Samyn, A. Persson, and A. Svensson. Relation between neighbouring grains in the upper part of the northgrip ice core - implications for rotation recrystallization. *Earth Planet. Sci.*, 2007. *Submitted*.

- [33] O. Castelnau, Th. Thorsteinsson, J. Kipfstuhl, P. Duval, and G. R. Canova. Modelling fabric development along the GRIP ice core, central Greenland. *Ann. Glaciol.*, 23:194–201, 1996.
- [34] S. De La Chapelle, O. Castelnau, V. Lipenkov, and P. Duval. Dynamic recrystallization and texture development in ice as revealed by the study of deep ice cores in Antarctica and Greenland. *J. Geophys. Res.*, 103(B3):5091–5105, 1998.
- [35] P. Duval. Creep and fabrics of polycrystalline ice under shear and compression. *J. Glaciol.*, 27(95):129–140, 1981.
- [36] T. H. Jacka and M. Maccagnan. Ice crystallographic and strain rate changes with strain in compression and extension. *Cold. Reg. Sci. Technol.*, 8:269–286, 1984.
- [37] Y. Wang and N. Azuma. A new automatic ice-fabric analyzer which uses image-analysis techniques. *Ann. Glaciol.*, 29:155–162, 1999.
- [38] D. S. Russell-Head and C. J. L. Wilson. Automated fabric analyser system for quartz and ice. *Geological Society of Australia*, 64:159, 2001. *Abstracts*.
- [39] L. A. Wilen, C. L. Diprinzio, R. B. Alley, and N. Azuma. Development, principles, and applications of automated ice fabric analysers. *Micro. Res. and tech.*, 62:2–18, 2003.
- [40] G. Durand, O. Gagliardini, T. Thorsteinsson, A. Svensson, J. Kipfstuhl, and D. Dahl-Jensen. Ice microstructure and fabric: an up to date approach to measure textures. *J. Glaciol.*, 52(179):619–630, 2006.
- [41] Y. Wang, S. Kipfstuhl, N. Azuma, T. Thorsteinsson, and H. Miller. Ice-fabrics study in the upper 1500 m of the Dome C (East Antarctica) deep ice core. *Ann. Glaciol.*, 37(1):97–104, 2003.
- [42] M. Gay and J. Weiss. Automatic reconstruction of polycrystalline ice microstructure from image analysis: application to the EPICA ice core at Dome Concordia, Antarctica. *J. Glaciol.*, 45(151):547–554, 1999.
- [43] N. H. Woodcock. Specification of fabric shapes using an eigenvalues method. *Geol. Soc. Am. Bull.*, 88:1231–1236, 1977.
- [44] O. Gagliardini, G. Durand, and Y. Wang. Grain area as a statistical weight for polycrystal constituents. *J. Glaciol.*, 50(168), 2004.
- [45] J. Weiss, J. Vidot, M. Gay, L. Arnaud, P. Duval, and J. R. Petit. Dome concordia ice microstructure: impurities effect on grain growth. *Ann. Glacio.*, 35:552–558, 2002.
- [46] EPICA Community members. Eight glacial cycles from an Antarctic ice core. *Nature*, 429:623–628, 2004.
- [47] G. Durand, F. Gillet-Chaulet, A. Svensson, O. Gagliardini, S. Kipfstuhl, J. Meyssonier, F. Parrenin, P. Duval, and D. Dahl-Jensen. Change in ice rheology during climate variations - implications for ice flow modeling and dating of the EPICA dome C core. *Clim. Past*, 2006. *In Press*.
- [48] M. J. Gore, M. Grujicic, G. B. Olson, and M. Cohen. Thermally activated grain boundary unpinning. *Acta Metall.*, 37(11):2849–2854, 1989.
- [49] F. Parrenin and J.-M. Barnola, J. Beer, T. Blunier, E. Castellano, J. Chappellaz, G. Dreyfus, H. Fischer, S. Fujita, J. Jouzel, K. Kawamura, B. Lemieux-Dudon, L. Louergue, V. Masson-Delmotte, B. Narcisi, J.-R. Petit, G. Raisbeck, D. Raynaud, U. Ruth, J. Schwander, M. Severi, R. Spahni and J.P. Steffensen, A. Svensson., R. Udisti, C. Waelbroeck, and E. Wolff. The ED3 agescale for the EPICA dome C ice core. *Cl. Past.*, 2007. *In press*.
- [50] T. H. Jacka and J. Li. The steady-state crystal size of deforming ice. *Annals of Glaciology*, 20:13–18, 1994.
- [51] M. Jessell, P. Bons, L. Evans, T. Barr, and K. Stüwe. Elle: the numerical simulation of metamorphic and deformation microstructures. *Comp. geosc.*, 27:17–30, 2001.
- [52] C. L. Diprinzio, L. A. Wilen, R. B. Alley, J. J. Fitzpatrick, M. K. Spencer, and A. J. Gow. Fabric and texture at Siple dome, Antarctica. *J. Glaciol.*, 51(173):281–290, 2005.
- [53] J. F. Nye. The topology of ice-sheet centres. *J. Glaciol.*, 37:220–227, 1991.
- [54] F. Rémy and I. E. Tabacco. Bedrock features and ice flow near the EPICA ice core site (Dome C, Antarctica). *Geophys. Res. Lett.*, 24(3):405–408, 2000.
- [55] G. B. Dreyfus, F. Parrenin, B. Lemieux-Dudon, G. Durand, V. Masson-Delmotte, J. Jouzel, J. M. Barnola, L. Panno, R. Spahni, A. Tisserand, U. Siegenthaler, and M. Leuenberger. Anomalous flow below 2700 m in the EPICA Dome C ice core detected using  $\delta^{18}\text{O}$  of atmospheric oxygen measurements. *Clim. Past.*, 2007. *In Press*.